ISSN 1027-4510, Journal of Surface Investigation: X-ray, Synchrotron and Neutron Techniques, 2023, Vol. 17, No. 6, pp. 1463–1471. © Pleiades Publishing, Ltd., 2023.

Excitation of Terahertz Plasmonic Resonance on a Subwavelength Metallic Grating in an Attenuated Total Reflection Scheme Using a Monochromatic Radiation Source

O. E. Kameshkov[a, b, *] and V. V. Gerasimov[a, b]

[a] *Budker Institute of Nuclear Physics, Siberian Branch, Russian Academy of Sciences, Novosibirsk, 630090 Russia*

[b] *Novosibirsk National Research State University (NSU), Novosibirsk, 630090 Russia*

**e-mail: o.kameshkov@g.nsu.ru*

Received April 14, 2023; revised June 24, 2023; accepted June 24, 2023

Abstract—Sensors based on surface plasmon resonance excited in the scheme of attenuated total reflection (ATR) on thin metal films have undergone a revolution in the visible frequency range. It is possible to study very weak interactions, up to single molecules, using these sensors. Such an approach, which has already become classical, cannot be implemented in the terahertz-frequency range. Terahertz waves barely penetrate metals due to their high dielectric constant, which makes it difficult to maintain resonance at the metal–dielectric interface. One way to overcome this problem is to modify the metal surface with a structure with a characteristic size much smaller than the radiation wavelength. The structured region of the metal behaves as an effective layer of the medium, the permittivity of which is a function of the response of the dielectric and the metal. On these structures, spoof-surface plasmon resonances, which are similar in properties to surface plasmon resonances in the visible range, can be excited. By combining spoof-surface plasmon resonance and attenuated total reflection, it is possible to implement a sensor that, in the future, will make it possible to detect the smallest concentrations and observe small changes in the boundary dielectric medium in the terahertz-frequency range. The excitation of a spoof-surface plasmon resonance is studied using the method of attenuated total reflection on a flat one-dimensional subwavelength grating with gold sputtering in the Otto scheme. For the first time, the angular reflection spectra are measured according to this scheme using monochromatic terahertz radiation from the Novosibirsk free-electron laser (the wavelength is 141 μm). The plasmon resonances observed in the spectra are consistent with the simulation results using COMSOL Multiphysics.

Keywords: spoof-surface plasmon resonance, subwavelength grating, attenuated total reflection, sensor, terahertz radiation, Novosibirsk free-electron laser

DOI: 10.1134/S1027451023060290

INTRODUCTION

Terahertz (THz) spectroscopy is an alternative technology for the detection of biomaterials. THz waves have a low energy (several meV) that is lower than the ionization energy of atoms and molecules, which makes it possible to analyze materials without destroying the studied medium. The frequency range of THz waves correlates with the vibrational frequencies of many important biomolecules in the gas phase (proteins, RNA, and DNA), which makes it possible to recognize their vibrational and rotational spectra. All this makes THz technologies suitable for contactless, marker-free, repeatable, and selective methods for measuring and detecting biological objects. However, a low spatial resolution due to the large wavelength and strong absorption by polar liquids create many problems for the use of THz radiation in biological problems [1].

To solve these problems, surface plasmon polaritons, which are collective oscillations of electrons propagating along the metal–dielectric interface, are often used [2]. They make it possible to improve the recognition of molecular spectral responses and to implement so-called field-enhanced spectroscopy. The operating principle of this technology is based on amplification of the electromagnetic near field near a metal surface at a certain frequency to enhance the absorption of waves by samples attached to the surface.

The appearance of surface plasmon polaritons at the metal—dielectric interface and their properties are related to the permittivity of metals. The negative permittivity leads to the appearance of evanescent waves at the metal–dielectric interface, which penetrate both the metal and the dielectric. However, plasmons that are well localized and bound to the metal surface exist only in the visible and near-infrared frequency ranges. In the low-frequency region, metals behave

almost as ideal electrical conductors and, thus, only a small fraction of the electric fields of plasmon polaritons penetrate into the metal, which leads to the weak coupling of plasmons with the metal surface and their scattering into bulk waves even at a slight roughness or optical heterogeneity [3].

One of the ways to overcome this problem is periodic structuring of the metal [4], and its simplest implementation is a subwavelength periodic grating. When the grating period is much smaller than the electromagnetic wavelength, the grating behaves as an effective layer of the medium, whose dielectric function mixes the responses of the metal and the dielectric environment of the grating. The effective dielectric function of the grating can be described by the Drude model, but with a much lower plasma frequency compared to a real metal [5]. Such structures support highly confined spoof-plasmon modes similar to classical surface plasmon polaritons (spoof-surface waves imitate the properties of classical surface waves, but they are described by completely different dispersion equations). By means of these modes, it is possible to enhance the electromagnetic coupling of a metal with a dielectric. Sensors based on them can be tuned in angle or frequency. All this makes it possible to amplify selectively the vibrational responses of the studied molecules using these structures.

Sensors based on spoof-surface plasmon resonance (SSPR) are rather often mentioned in publications, and their properties have been studied extensively. Ng Binghao et al. [6] were the first to experimentally determine the refractive indices of nitrogen and various liquids by tracking changes in the sharp peaks of the SSPR in the amplitude and phase THz spectra using the method of time-domain spectroscopy [6]. They achieved sensitivity for nitrogen by shifting the frequency resonance of $S \approx 0.49$ THz/RIU (RIU is the refractive-index unit), the quality factor of $FOM \approx 49$ RIU^{-1}, and the refractive-index sensitivity of $\Delta n = 0.02$ RIU. In [7], the fundamental mode and higher-order SSPR modes excited on metal gratings with various groove depths and other fixed parameters were compared numerically. High-order modes had a higher sensitivity (up to 2.27 THz/RIU) and Q factor ($FOM \approx 262$ RIU^{-1}) with $\Delta n = 0.004$ RIU. The effect of the gap between the prism and the subwavelength grating on the resonance depth was also studied. In [8], the plasmon resonances were numerically studied in the angular spectrum at 1 and 0.8 THz. In the case of a silicon prism and a rectangular gold grating, an extremely high angular sensitivity ($S = 320$ deg/RIU) was achieved, corresponding to a refractive-index resolution of $\Delta n = 3 \times 10^{-7}$ RIU, which is comparable to the characteristics of similar sensors in the visible frequency range. By changing the slope of the rectangular grooves, a sensitivity of $S = 452$ deg/RIU was achieved [8]. The effect of the incident angle of radiation on the sensitivity of sensors and the range of determination of the refractive index was theoretically studied in [9]. A smaller angle of incidence resulted in a higher sensitivity of sensors with a narrower detection range. In [10], subwavelength gratings were considered as a liquid sensor. Using numerical simulation, the effect of the shape of the grating grooves (trapezium, triangle, and rectangle) and the position of the liquid relative to the grooves (the liquid completely fills the gap and grooves; the liquid fills the grooves only) on resonance was studied. The possibility of operating this type of sensor in the Otto scheme for studying polar liquids was experimentally considered in [11], and the same authors used phase spectral analysis in [12]. Liquid sensors were studied in [13]. The specific feature of the study is that a new form of grooves for subwavelength gratings, which are easy to manufacture was proposed. In [14], the analytical theory of the condition for matching wave vectors in a scheme with subwavelength gratings in the Otto configuration, in which the error is caused by the refractive index of the sample, was refined. Both studies [13, 14] are based on numerical analysis. The question of the spectral analysis of molecules using these structures was raised in [15].

Basically, all experimental work with sensors based on SSPR was performed using a broadband source in the course of measuring frequency spectra while no experimental work, in which angular spectra were obtained, was found. In this study, we experimentally study the angular spectra of SSPR obtained by the method of Attenuated total reflection (ATR) in the Otto scheme using THz radiation of the Novosibirsk free-electron laser.

THEORY OF SSPR EXCITATION ON SUBWAVELENGTH GRATINGS BY THE ATR METHOD

When a plane wave is incident on the interface between a prism (with the refractive index n_p) and a dielectric (with the refractive index n_d), the wave is partially reflected and partially transmitted. At a rather large angle of $\theta_{int} > \theta_{cr} = \arcsin(n_d/n_p)$, there is no refracted wave, and total internal reflection occurs. Despite the fact that such a reflection is called total, an evanescent electromagnetic wave attenuating with distance arises in an optically less dense sample.

In the angular reflection spectrum, as the critical angle is approached, a gradual increase in the reflection coefficient is observed, with subsequently reaching a plateau in the region of the critical angle with the

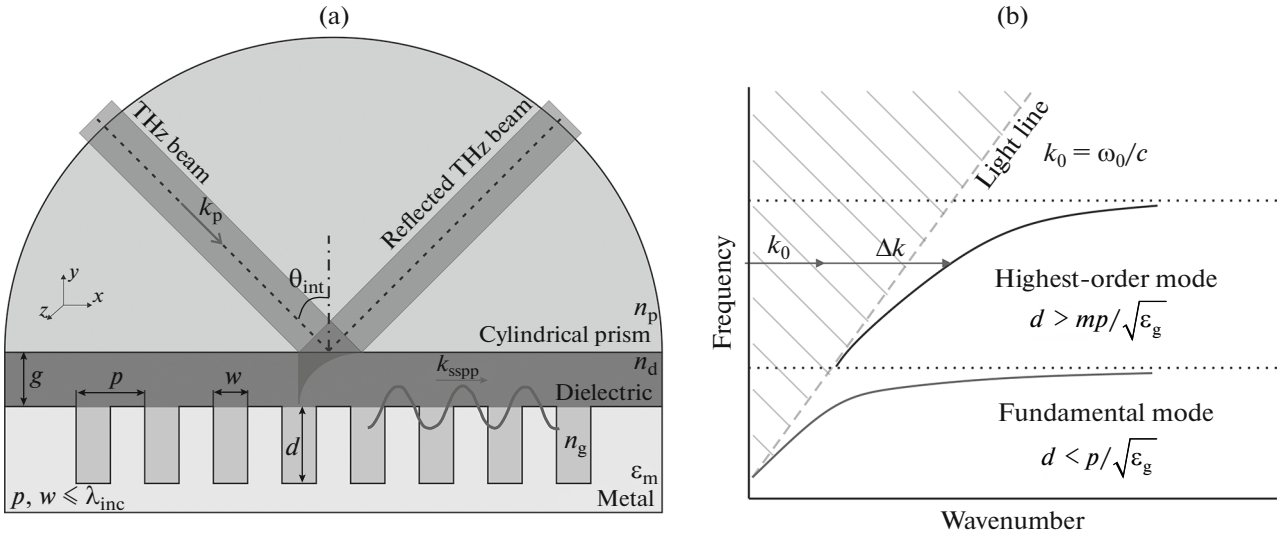

Fig. 1. (a) Physical formulation of the problem: the process of excitation of spoof-surface plasmon polaritons on a subwavelength grating by the ATR method in the Otto configuration is shown. (b) Qualitative demonstration of the dispersion curve of spoof-surface plasmon polaritons.

maximal value of the reflected energy. This phenomenon is described using the Fresnel formulas:

$$r_{TE} = \frac{n_p \cos\theta_{inc} - n_d \cos\theta_{cr}}{n_p \cos\theta_{inc} + n_d \cos\theta_{cr}}, \quad R = |r|^2,$$
$$r_{TM} = \frac{n_d \cos\theta_{inc} - n_p \cos\theta_{cr}}{n_p \cos\theta_{cr} + n_d \cos\theta_{inc}}, \qquad (1)$$
$$\theta_{cr} = \arcsin\left(\frac{n_d \sin(\theta_{inc})}{n_p}\right).$$

To excite SSPR on subwavelength metal gratings, we use the ATR method in the Otto configuration (Fig. 1a). A THz beam with transverse magnetic (TM) polarization in a semicylindrical prism illuminates the boundary between the prism and the dielectric at an incidence angle of $\theta_{int} > \theta_{cr}$, producing an evanescent wave that interacts with a subwavelength metal grating. After interaction with the analyte and the grating, the light is reflected and recorded. If the $\mathbf{k}_p$ projection of the incident wave in the prism onto the abscissa axis is aligned with the $\mathbf{k}_{SSPP}$ vector of the spoof-surface plasmon propagating along the grating, then the wave-vector matching condition will be satisfied. The damped evanescent wave will be associated with SSPR, and a dip in the reflection spectrum will be observed:

$$k_x = k_p \sin(\theta_{int}) = \frac{2\pi}{\lambda}\frac{n_p}{n_d}\sin(\theta_{int}) = k_{SSPR}, \qquad (2)$$

where λ is the wavelength in free space. A one-dimensional grating with the period p, stroke width w, and depth d can be modeled (in the limit, $p, w, d \ll \lambda$) as a dielectric layer with an effective permittivity that depends on the grating parameters. Given the losses in the metal, the wave vector of the surface plasmon polariton k_{SSPP} can be written as follows [16]:

$$k_{SSPR} = \left(\varepsilon_d k_0^2 + \left(\frac{w\varepsilon_d}{p\varepsilon_g}\right)^2 k_g^2 \tan^2(k_g d)\right)^{1/2}, \qquad (3)$$

where $k_g = k_0\sqrt{\varepsilon_g}\left(1 + l_s(i+1)/w\right)^{1/2}$ is the wave vector in the groove, ε_d and ε_g are the permittivity of substances in the gap and grooves, respectively; $k_0 = 2\pi/\lambda$ is the wavenumber of a wave in free space, and $l_s = \left(k_0 \operatorname{Re}\sqrt{-\varepsilon_m}\right)^{-1}$ is the skin-layer thickness of metal with the permittivity ε_m.

Expression (3) is the dispersion relation for SSPRs propagating along a subwavelength grating. Wave vector k_{SSPP} is highly dependent on the structure parameters, which provides flexibility in designing gratings for sensor applications. It is worth noting that the wave vector of a surface wave propagating along a corrugated surface is limited by the first Brillouin zone of $k_x < \pi/p$. Thus, according to (1) and (2), only the fundamental mode can be excited at $d < p/\sqrt{\varepsilon_g}$ while at $d > mp/\sqrt{\varepsilon_g}$ (m is the order of the mode), the grating can support modes of a higher order ($m = 1, 2, 3, \ldots$). An illustrative dispersion curve of a subwavelength grating is shown in Fig. 1b.

SIMULATION WITH COMSOL

In this study, we performed numerical simulations using the finite difference method and commercially available COMSOL Multiphysics software. In COMSOL, the first step was to calculate the dispersion curves and

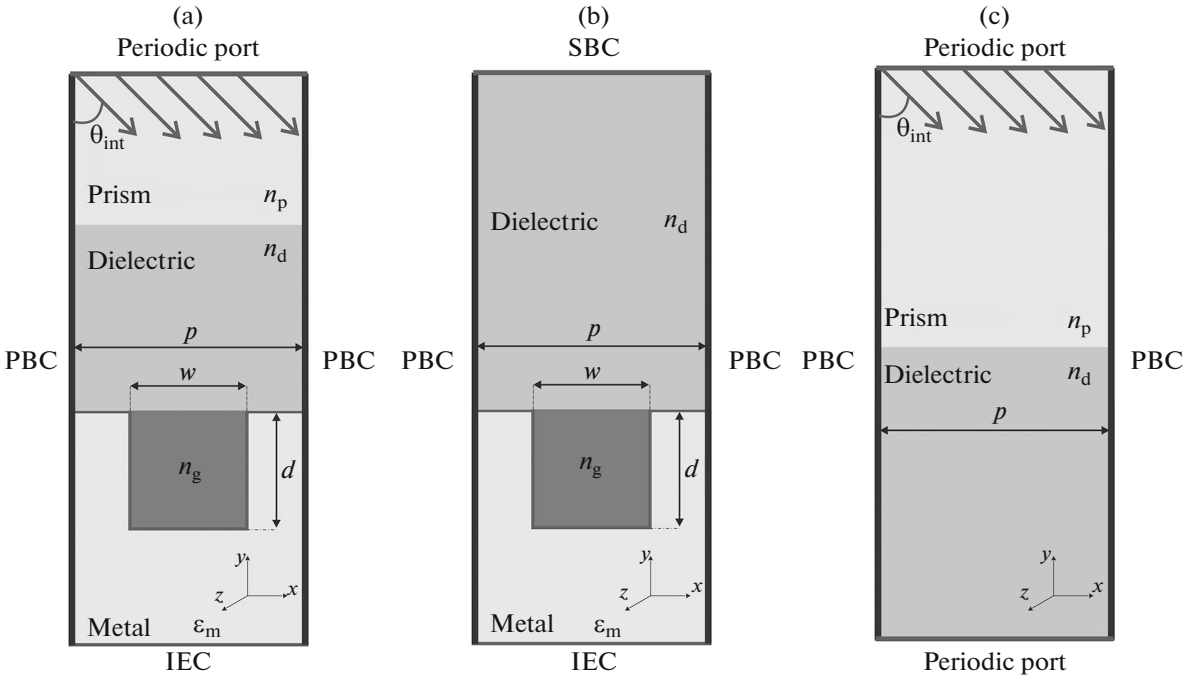

Fig. 2. Numerical scheme in COMSOL: (a) to search for eigenmodes, (b) to calculate the angular and frequency reflection spectra, and (c) for modeling the incidence of a plane wave on the boundary of two media (without grating). PBC is a periodic boundary condition, SBC is a scattering boundary condition, and IEC is an ideal electrical conductor.

select the required resonance frequency and angle. At the second stage, the gap size was optimized for the effective excitation of SSPR by the Otto method. For further comparison with the experiment, the incidence of a plane wave on the prism–dielectric interface without a grating was simulated.

Calculation of the Dispersion Curve

When analyzing modes and eigenfrequencies, the main problem is usually to find the propagation constant or eigenfrequency. In COMSOL, there is an eigenfrequency analyzer that solves the electromagnetic-field problem as $\mathbf{E}(\mathbf{r},t) = \mathrm{Re}\left(\tilde{\mathbf{E}}(\mathbf{r})\exp(-\lambda t)\right)$, where the complex eigenvalue of $\lambda = -\delta + i\omega$ has the imaginary part ω (eigenfrequency) and real part δ responsible for attenuation.

The COMSOL eigenmode solver was used to excite the eigenmodes. Its main feature is the possibility of the excitation of eigenmodes without an external source. This program was used to analyze spoof-plasmon modes on subwavelength metallic linear rectangular gratings in a 2D formulation (Fig. 2a). In this case, the right and left boundaries of the Floquet cell were periodic. The component of wave vector k_x directed along the surface varies. An eigenmode is excited when k_x coincides with the propagation constant. To completely determine the computational domain, the upper boundary was found using the scattering boundary condition while the lower boundary was found using the impedance boundary condition [17].

Calculation of Angular and Frequency Spectra

The scheme of the numerical experiment for the calculation of angular spectra in COMSOL (Radio Frequencies module) is shown in Fig. 2b. The left and right boundaries of the Floquet cell are determined using periodic boundary conditions: the Floquet conditions. Applying this condition means that the solution on one side of the cell is equal to the solution on the other side times the complex phase factor. The phase shift between the boundaries is estimated from the perpendicular component of the wave vector k_x. The port is also periodic and excites a plane TM wave of $(H_x\ H_y\ H_z) = (0\ 0\ 1)$. The permittivity of the metal was modeled using the Drude model: $\varepsilon = 1 - \dfrac{\omega_p^2}{\omega^2 + i\omega\omega_\tau}$, where ω_τ is the electron-collision frequency, and ω_p is the plasma frequency. The frequency was fixed while the incidence angle θ was varied during the calculation. Beam reflection from the prism–dielectric interface (Fig. 2c) in the absence of a grating under the prism was also simulated using the Radio Frequencies module (COMSOL). A receiving periodic port was set to close the numerical scheme at the lower boundary of the Floquet cell.

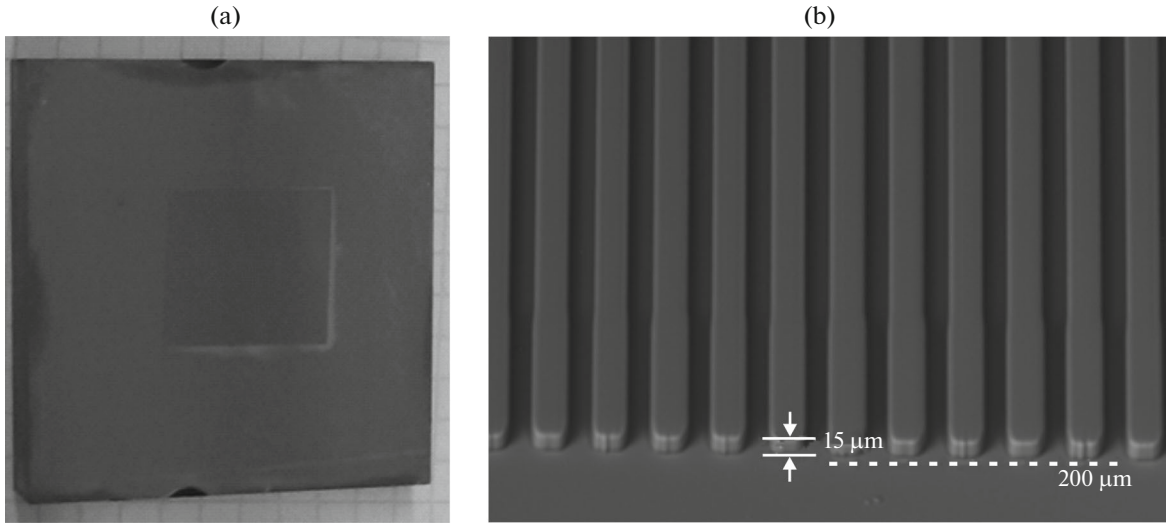

Fig. 3. Images of the sample: (a) general view, (b) in a microscope.

Simulation Results

For modeling and experiments, the available subwavelength grating with gold sputtering fabricated by the method of projection X-ray lithography [18] was taken. This grating was previously used as a waveguide spoof-plasmon sensor [19]. The substrate for the grating was a polished plane-parallel glass plate, on which an SU-8 photoresist was applied. The resist was exposed to synchrotron radiation through an X-ray mask at the LIGA station, Budker Institute of Nuclear Physics, Siberian Branch, Russian Academy of Sciences. The deviation of the geometric dimensions of the samples did not exceed 1 μm. The grating (Fig. 3) had the following parameters: $p = 40$ μm, $w = 14.5$ μm, and $d = 19$ μm.

Figure 4 shows the analytical and numerical dispersion curves for this grating. It is of interest to work at one of the frequencies generated by the Novosibirsk free-electron laser, $f_{res} = 2.126$ THz (141 μm), which lies in the transparency window of THz radiation. As can be seen, the numerical dispersion curve is located below the analytical one, and, as a result, resonance occurs at an angle of 18.8° rather than 18.27°, which is close to the critical ATR angle of $\theta_{cr} = \arcsin(1/3.42) = 17°$.

The differences between the analytical dispersion curve and the numerical one are related to the effective medium model, in which the equations for the wave vector of spoof plasmons are obtained. The model does not take into account higher diffraction orders arising on a subwavelength grating, as well as the interaction of fields arising above the grating grooves. These effects can be taken into account using a more rigorous subwavelength grating model [20] or by numerical simulation, which is chosen as the basis.

At the next stage, the optimal gap g was selected by the angular reflection spectra. Before calculations, based on the analysis of mesh convergence, the mesh size in the vicinity of the metal–dielectric interface was chosen to be 0.2–0.5 μm, which is slightly larger than the skin-layer depth in the THz frequency range. At a smaller mesh size, the accuracy of calculations increased slightly while the calculation time increased many times over. The optimization result (Fig. 5) is presented as a two-dimensional graph of the distribution of the reflection coefficient over the gap size and the incidence angle. As can be seen, the maximal dip

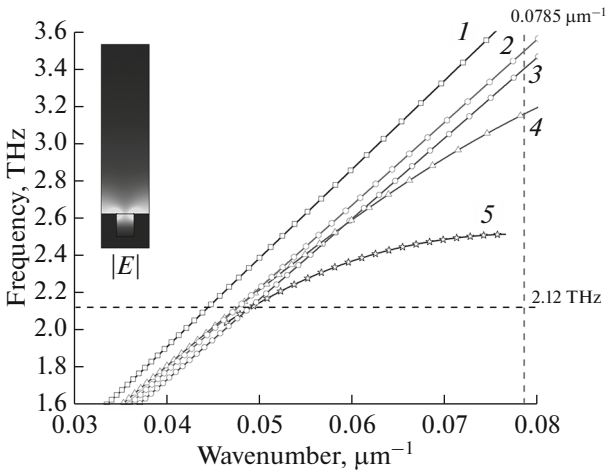

Fig. 4. (*1*) Dispersion curves k_0 (light line) and k_x in the case of resonance at (*2*) 18.27° and (*3*) 18.8°; (*4*, *5*) analytical and simulated $\mathrm{Re}\{k_{SSPP}\}$ curves, respectively. Resonance must be observed at 2.126 THz at an angle of 18.8° for the numerical dispersion curve *3* and at 18.27° for analytical curve *2*. The dispersion curve is limited along the *Oy* axis: $p < 40$ μm (7.5 THz) and the *Ox* axis by the first Brillouin zone: $k < \pi/40 = 0.0785$ μm^{-1}. The inset shows the distribution of the electric-field norm of the spoof-plasmon mode.

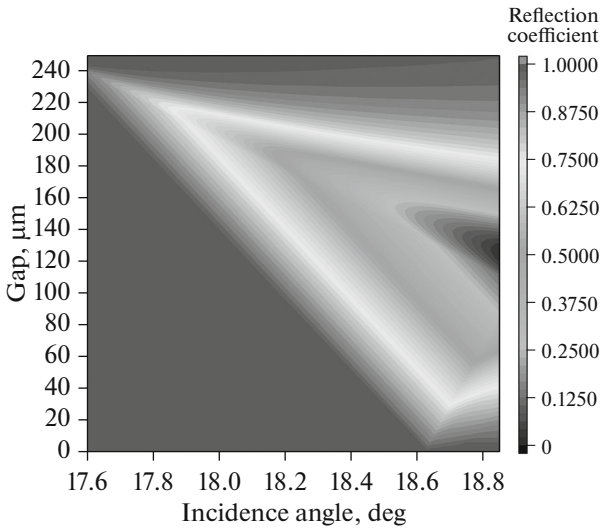

Fig. 5. 3D distribution of gap g over incidence angle θ and the reflection coefficient.

depth is observed at a gap of 120 μm and a frequency of 2.126 THz.

EXPERIMENTAL

Experimental Setup

For the experiment, the scheme shown in Fig. 6 was assembled. The incident power of the THz beam of the Novosibirsk free-electron laser was controlled using a film polarizer. Using a system of mirrors and a splitter, part of the beam energy was directed to a reference optoacoustic detector (Golay cell), which was used to control the laser power. The other part passed through a system consisting of a diaphragm, a polarizer, and a telescopic system (two lenses with the focal lengths f_1 and f_2, reducing the beam size by a factor of f_1/f_2) and hit a prism with a grating on the reverse side. The polarizer in the experiment singled out two specific directions of the electric-field vector of the incident radiation: TM (**E** ⊥ grating grooves) and transverse electric (TE) (**E** ∥ grating grooves). The beam reflected from the interface (prism—air–grating) was recorded using the main Golay cell. Since the used receivers can record only a variable radiation flux, the input beam was modulated by a mechanical obturator at 30 Hz. The signals from the outputs of the receivers were recorded using two synchronous detectors (Stanford Research 830).

The prism position, which specifies the incidence angle of the beam, the position of the grating relative to the prism, which determines the gap between the prism and the grating, and the position of the main detector were adjusted using a system of automated movements. Movement control, as well as the collection and processing of signals from synchronous detectors, was carried out using a specially developed program using Labview.

RESULTS

Spectra of Total Internal Reflection

Initially, the angular reflectance spectra were measured in the absence of a sample behind the prism to test the condition of total internal reflection (TIR). The spectra were normalized first to the reference signal and then to the maximal value (since the reflection

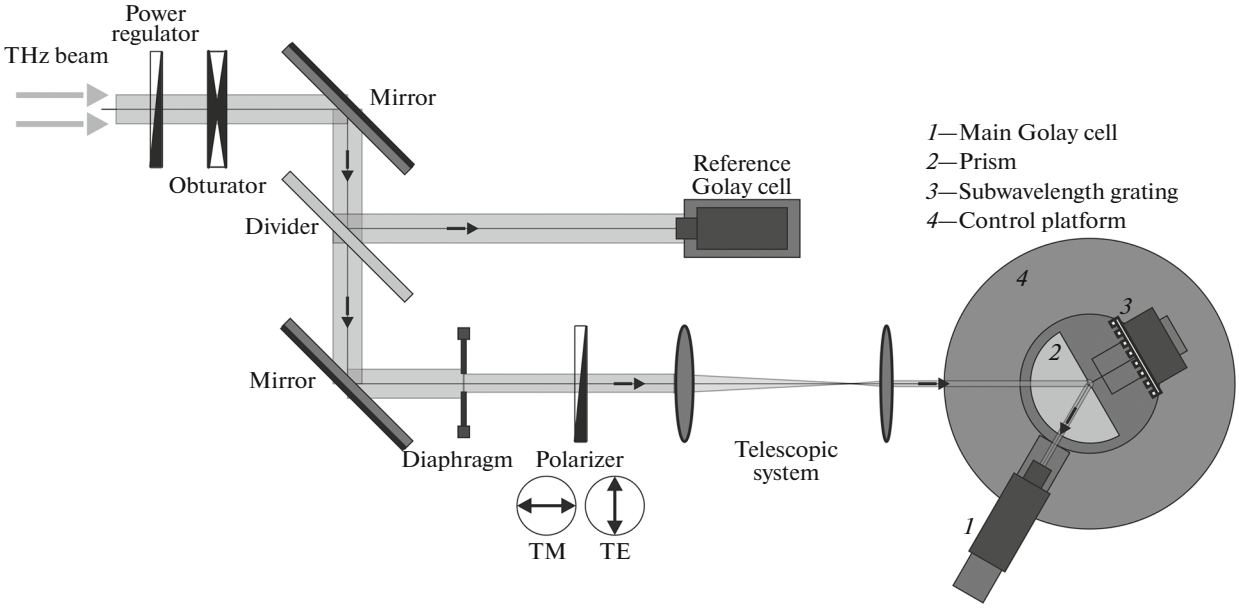

Fig. 6. Experimental scheme.

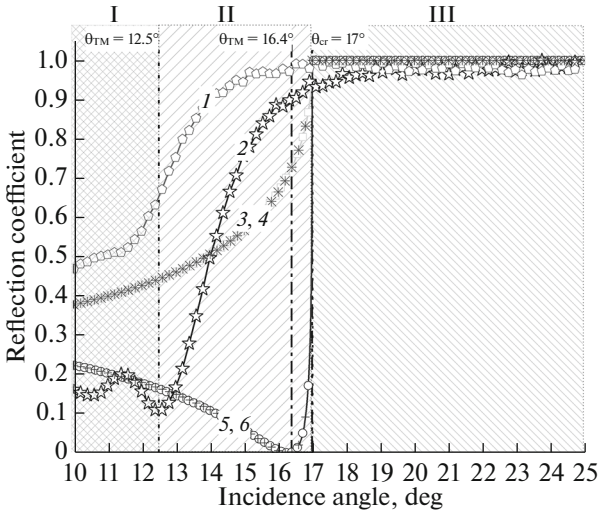

Fig. 7. Comparison of ATR spectra obtained in (*1*, *2*) the experiment with (*3*, *5*) analytical and (*4*, *6*) numerical results: (*1*, *3*, *4*) TE wave, (*2*, *5*, *6*) TM wave. The dashed lines show the experimental regions described in the text for the TM-polarized wave.

coefficient cannot exceed unity). The experimental graphs obtained in this way for TM and TE waves, as well as numerical and analytical calculations, are shown in Fig. 7.

Due to the rather large radiation wavelength (0.14 mm), the diffraction and interference effects that occur on elements of the optical scheme (telescope, diaphragm, and prism) significantly affected the angular spectra: they differ markedly from the theoretical curves. Of particular interest are the results for the TM wave since SSPR must be excited precisely at this polarization. On the experimental graph for the TM wave (Fig. 7), three ranges of angles can be distinguished: the first (10°–12.5°) corresponds to the transmission and reflection of a part of the radiation at the prism–air interface; in the second (12.5°–17°), the reflection coefficient increases steadily; and the third (more than 17°) corresponds to the TIR region, where the signal plateau is observed, and the entire signal is a reflected wave. The last TIR region always begins after $\theta_{cr} = 17°$, which is consistent with the theory. The boundaries of the first and second regions differ greatly from the theoretical ones (up to 4°), which can be explained by diffraction and interference effects in the optical scheme.

Reflection Spectra from a Smooth Metal Surface

When the subwavelength grating is located near the prism at some distance, besides the conversion of a part of the energy of the evanescent wave into SSPR, interference effects can be observed in the angular spectrum, especially at incidence angles less than the critical one. To separate these effects from the excitation of the plasmon resonance, experiments with a metal mirror arranged in place of the grating were performed (Fig. 8). Indeed, at incidence angles smaller than the critical one, interference dips and signal maxima are observed in the spectra in both cases of polarization while the dips deepen as the gap increases. At angles greater than the critical one, TIR occurs in the prism.

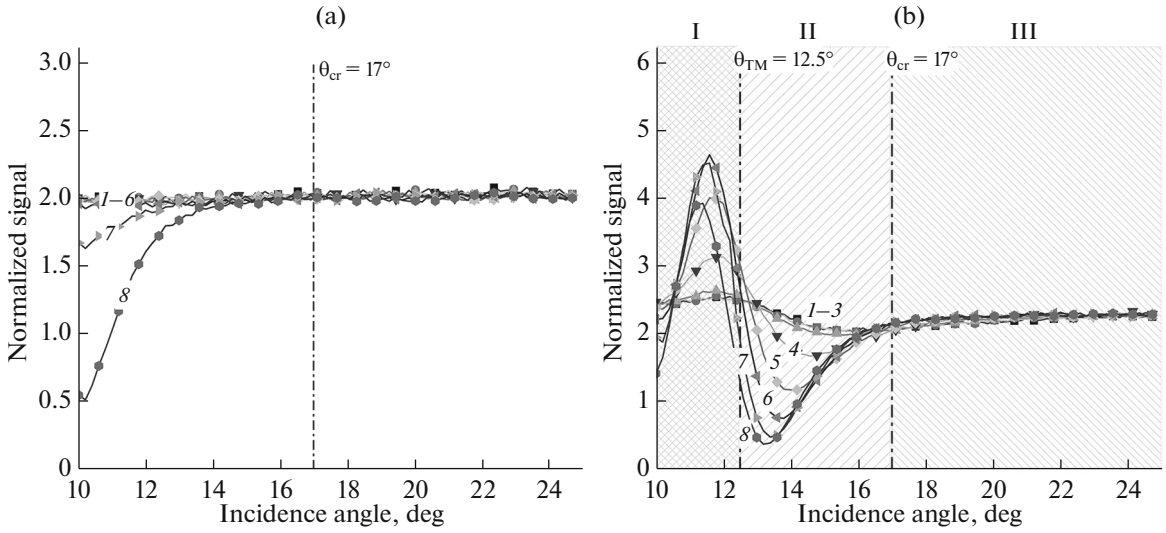

Fig. 8. Angular reflection spectra in the ATR scheme with a reflecting surface at (a) TE and (b) TM polarization and a gap of: (a) (*1–6*) 80, 100, 120, 140, 160, 180, (*7*) 200, and (*8*) 220 μm; (b) (*1–3*) 80, 100, 120, (*4*) 140, (*5*) 160, (*6*) 180, (*7*) 200, and (*8*) 220 μm.

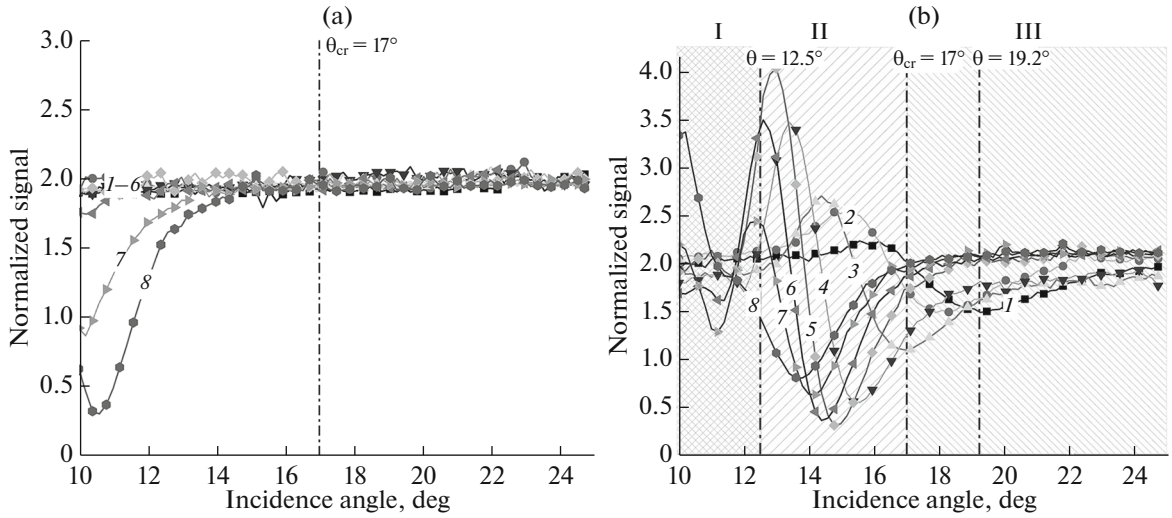

Fig. 9. Angular reflection spectra in the ATR scheme with a subwavelength grating at (a) TE and (b) TM polarization and a gap of: (a) (*1*–*6*) 80, 100, 120, 140, 160, 180, (*7*) 200, and (*8*) 220 μm; (b) (*1*) 80, (*2*) 100, (*3*) 120, (*4*) 140, (*5*) 160, (*6*) 180, (*7*) 200, and (*8*) 220 μm.

Reflection Spectra from a Subwavelength Grating

In the experiment with a subwavelength grating (Fig. 9), strong interference dips and maxima were also observed for both types of polarization, which made it difficult to distinguish the spoof-plasmon dip. As was shown above, all the effects that arise up to a critical angle of $\theta = 17°$ (the first and second regions) cannot be associated with the excitation of SSPR. In the region of angles greater than the critical one, in the case of TM polarization, small dips were observed at a gap of 80, 100, and 120 μm, which were absent in the case of TE polarization. This indicates the "plasmon-resonance nature" of these dips. For a gap of 80 μm, the resonance angle was 19.2°, which practically coincides with the numerical result (18.8°). A small difference could be due to the inaccuracy of establishing parallelism between the plane of the grating and the prism, as well as the error in determining the zero gap. As the gap increased, the plasmon resonances shifted towards smaller angles. As can also be seen, the width of SSPR in the experiment is much larger than that in numerical calculations, which may be due to diffraction broadening of the beam, dispersion of the grating parameters, and also large ohmic losses in the metallic layer of the grating.

CONCLUSIONS

In this study, for the first time, experiments on the excitation of spoof-plasmon resonances on a subwavelength one-dimensional metal grating were carried out using the TIR scheme on monochromatic THz radiation of the Novosibirsk free-electron laser. An analysis of the results showed that resonances are excited, but are strongly broadened in comparison with the results of numerical simulation due to beam diffraction on elements of the optical scheme. The inaccuracy in determining the zero gap between the prism and the grating, as well as their nonparallelism, could lead to a small resonance shift. In future studies, it is planned to improve the quality of the experimental angular spectra by replacing the telescopic system with a single lens, placing it in such a way that the prism—air–grating interface is in the region of the lens focus. To determine more accurately the gap and position of the grating relative to the prism, a prism made of a material that is transparent both to THz radiation and to visible light will be used, which will make it possible to implement alignment methods in visible light.

ACKNOWLEDGMENTS

The work was done at the shared research Siberian Synchrotron and Terahertz Radiation Center on the basis of the "Novosibirsk Free-Electron Laser Facility" at Budker Institute of Nuclear Physics of Siberian Branch Russian Academy of Sciences.

CONFLICT OF INTEREST

The authors declare that they have no conflicts of interest.

REFERENCES

1. Y. Peng, C. Shi, Y. Zhu, M. Gu, and S. Zhuang, PhotoniX **1**, 12 (2020).
2. S. A. Maier, *Plasmonics: Fundamentals and Applications* (Springer, New York, 2007).
3. V. V. Gerasimov, B. A. Knyazev, A. G. Lemzyakov, A. K. Nikitin, and G. N. Zhizhin, J. Opt. Soc. Am. B **33**, 2196 (2016). https://doi.org/10.1364/JOSAB.33.002196

4. J. B. Pendry, L. Martin-Moreno, and F. J. Garcia-Vidal, Science **305**, 847 (2004). https://doi.org/10.1126/science.1098999
5. M. Nazarov and J. L. Coutaz, J. Infrared, Millimeter, Terahertz Waves **32**, 1054 (2011). https://doi.org/10.1007/s10762-011-9814-5
6. B. Ng, J. Wu, S. M. Hanham, A. I. Fernandez-Dominguez, N. Klein, Y. F. Liew, M. Breese, M. Hong, and S. A. Maier, Adv. Opt. Mater **1**, 543 (2013). https://doi.org/10.1002/adom.201300146
7. H. Yao and S. Zhong, Opt. Express **22**, 25149 (2014). https://doi.org/10.1364/OE.22.025149
8. Y. Zhang, Z. Hong, and Z. Han, Opt. Commum. **340**, 102 (2015). https://doi.org/10.1016/j.optcom.2014.11.089
9. H. Yao, S. Zhong, and W. Tu, J. Appl. Phys. **117**, 133104 (2015). https://doi.org/10.1063/1.4916749
10. L. Chen, H. Yin, L. Chen, and Y. Zhu, J. Electromagn. Waves Appl. **32**, 471 (2018). https://doi.org/10.1080/09205071.2017.1395367
11. Y. Huang, S. Zhong, T. Shi, Y. Shen, and D. Cui, Opt. Express **27**, 34067 (2019). https://doi.org/10.1364/OE.27.034067
12. Y. Huang, S. Zhong, T. Shi, Y. Shen, and D. Cui, Nanophotonics **9**, 3011 (2020). https://doi.org/10.1515/nanoph-2020-0247
13. X. Chen, H. Xiao, G. Lu, and R. Zhao, J. Phys.: Conf. Ser. **1617**, 012008 (2020). https://doi.org/10.1088/1742-6596/1617/1/012008
14. R. Zhao, G. Lu, H. Yin, J. Liang, D. Zeng, and H. Xiao, Int. J. Antennas Propag. **2020**, 2504626 (2020) https://doi.org/10.1155/2020/2504626
15. H. Yao, W. Zhang, W. Liu, and H. Mei, J. Opt. **24**, 045301 (2022). https://doi.org/10.1088/2040-8986/ac5537
16. A. Rusina, M. Durach, and M. I. Stockman, Appl. Phys. A **100**, 375 (2010). https://doi.org/10.1007/s00339-010-5866-y
17. 17. Comsol RF Module User's Guide. Lossy Eigenvalue Calculations (2017).
18. B. G. Goldenberg, A. G. Lemzyakov, A. G. Zelinsky, V. P. Nazmov, and V. F. Pindyurin, J. Surf. Invest.: X-ray, Synchrotron Neutron Tech. **10**, 92 (2016). https://doi.org/10.1134/S1027451016010134
19. V. V. Bulgakova, V. V. Gerasimov, B. G. Goldenberg, A. G. Lemzyakov, and A. M. Malkin, Procedia Eng. **201**, 14 (2017). https://doi.org/10.1016/j.proeng.2017.09.638
20. M. Erementchouk, S. R. Joy, and P. Mazumder, Proc. R. Soc. A **472** (2195), 0160616 (2016). https://doi.org/10.1098/rspa.2016.0616

Translated by A. Ivanov